DESIGN AND OPTIMIZATION OF RENEWABLE ENERGY STRUCTURE

Nouha Nasri[1] and Souhir Tounsi[2]

[1]National School of Engineers of Gabès (ENIG), Gabès University, SETIT Research Unit, Sfax, Tunisia
[2]National School of Electronics and Telecommunications of Sfax, Sfax University, SETIT Research Unit, Sfax, Tunisia
Email: souhir.tounsi@enetcom.rnu.tn

Abstract: *Three important factors guarantee the performance of a generation chain of renewable energy are their efficiency, production cost and simplicity of the control algorithm to achieve a practical implementation in real time. Thus, three-generation chain structures of renewable energy are presented and studied in this paper for a selective comparative study to knowledge:*

- *Renewable Energy structure with DC-DC inverter elevator as protection system.*
- *Renewable Energy structure with excitation current regulator as protection system.*
- *Renewable Energy structure with regulated braking torque as protection system.*

These three types of energy generation chain are modeled simulation environment Matlab-Simulink. Simulation results encourage the choice of the generation chain with excitement current regulation system for its good efficiency, continuity of energy recovery than it is ranked the least expensive.

Key words: *Coiled Rotor Generator, Rectifier, Modeling, Battery, Braking Torque, DC-DC Inverter, Excitation System, Recovered Energy.*

1. Introduction

The choice of the power of chain structure and components fixed their efficiency, cost of production and the robustness of the control algorithm point of view electronic integration. In this context, several researches illustrate the advantages of asynchronous doubly fed machine as a solution for the generation of renewable energy such as low cost of asynchronous generator [1, 2]. However the asynchronous generation chains have multiple disadvantages such as their low ability to overcome current and power saw the interaction of the rotor and stator fluxes in a generally thin Air-gap generally causing deformation of the waveforms of current and forces electromotive, more these structure types have additional rotor losses and heavy monitoring algorithms and sometimes can not be integrated in real time [1, 2]. Structures with DC generators are simple but not robust given the magnetic armature reaction. The permanent magnet DC or AC generators are widely used, but have the drawback of a high cost connected to the cost of the magnets [3, 4]. To remedy to these problems our choice fell on a wound rotor generator with axial flux transferring energy to the battery energy storage in three configurations to be studied and presented in this paper in order to select the most efficient configuration based on the three criteria already mentioned. These three structures differ in their systems against overcurrent.

In this context, this paper presents three configurations of energy generation chains. A description of various modules of the three configurations also is presented. This study will be completed by a description of the implementation of the global models with their control algorithms in order to select the most efficient configuration.

2. Conversion Chain Structures

The first conversion chain (Figure 1) has a propeller to recover the energy generated by wind. This mechanical energy is converted into an alternating electrical energy via a gear speed amplifier and a coiled rotor synchronous generator. The electrical energy developed is also converted into DC power through a three-phase rectifier and a DC-DC elevator regulating the charging current continuously to the value 2600 A. The second power chain (Figure 2) has a propeller to recover the energy generated by wind. This mechanical energy is converted into an alternating electrical energy via a gear speed amplifier and a coiled rotor synchronous generator. It is equipped by an excitation current regulator maintaining the battery charging current constant equal to 2600 A via a DC-DC inverter.

The third conversion chain (Figure 3) has a propeller to recover the energy generated by wind. This mechanical energy is converted into an alternating electrical energy via a gear speed amplifier and a coiled rotor synchronous generator. The electrical energy developed is also converted into DC power through a three-phase rectifier. An automated braking system, piloted by pulse width modulation control, limits the charging current of the batteries to the value 2600 A to protect the energy

generation chain.

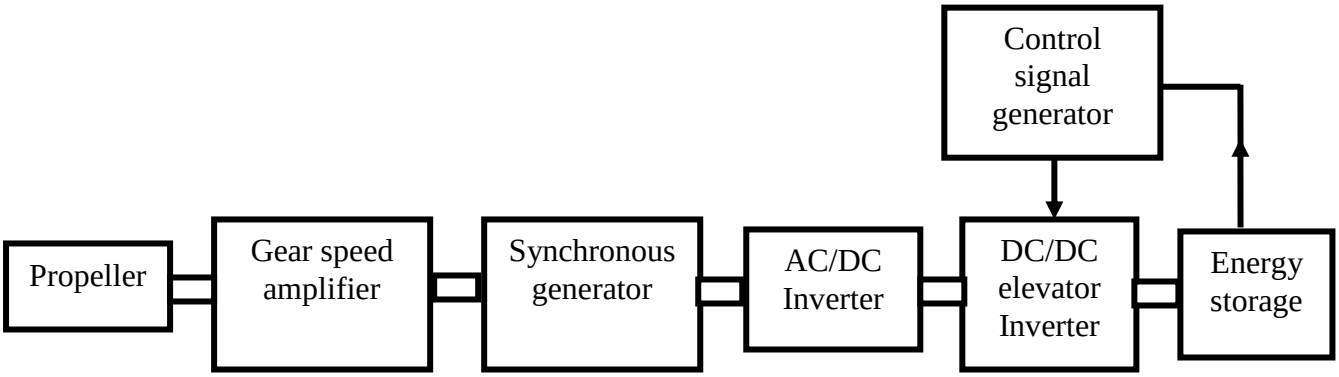

Fig.1. Structure of the power chain with current regulator

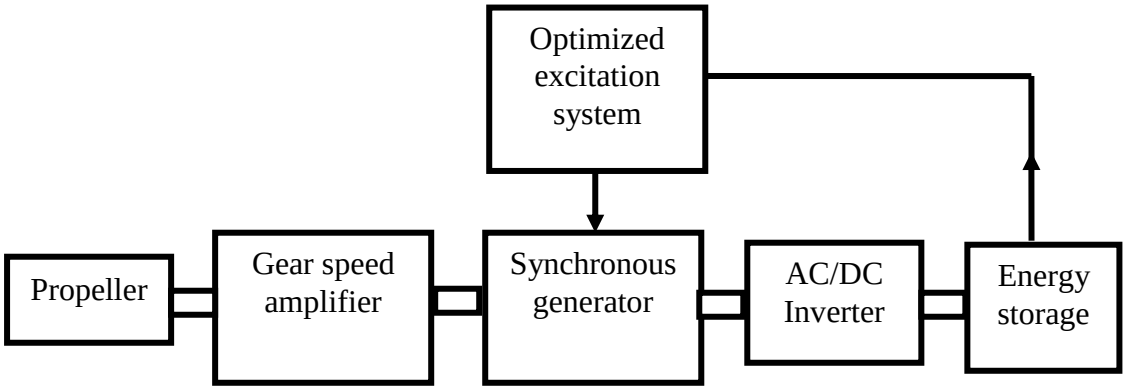

Fig.2. Structure of the power chain with excitation current regulator

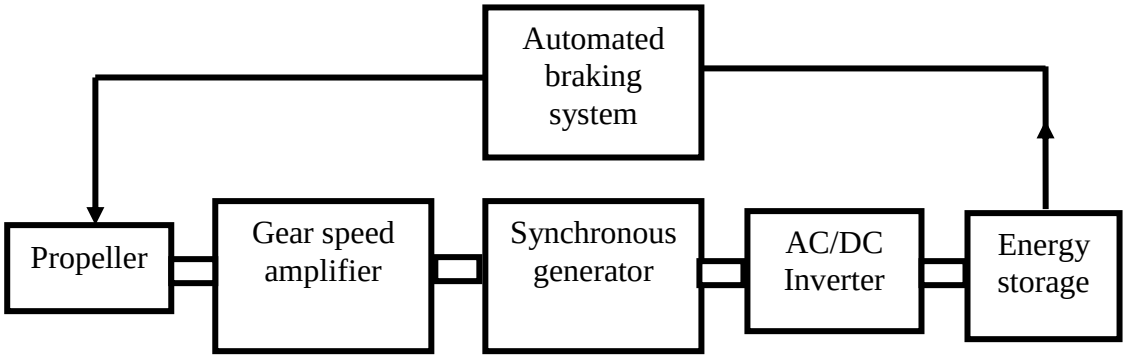

Fig.3. Structure of the power chain with braking system

3. Design of the synchronous generator

For designing the electric generator, our choice fell on the analytical method since it has the following key benefits [4-22]:

- It produces solutions quickly and without iterations.
- It provides acceptable precisions on the results because it is based on simplifying assumptions well argued and proper to address a design problem of an electrical device.
- It leads to highly parameterized design models leading to performance optimization.

The generator design problem by the analytical method is completely reversed to facilitate

resolution. Generally, we start from the generator dimensions to the power requirement and in this case a series of simulations is needed to converge to a satisfactory solution. In our case, we start from the generate power (maximum speed and maximum torque of the generator shaft) to the dimensions. The analytical method is set by the finite element simulations.

3.1. Generator structure

The generator is built with the same radius for the stator and the rotor. The slots directed towards the generator's center. Three coefficients define the structure of the generator.

- The first coefficient is the ratio β of the rotor coil average angular width by the pole pitch (L=π/p). It adjusts the rotor coil width in versus the poles number chosen.
- The second coefficient (α) is the ratio of the main tooth average angular width by the average angular width of the rotor coil. It adjusts the main tooth size

and has a strong influence on the electromotive force waveform.

- The last coefficient (r_{did}) fixes the inserted tooth size. It's the ratio of the main tooth average width by an inserted tooth average width.

The advantage of these coefficients is to define quickly machine shape. However, they are based on the average radius and it is necessary to compute and check higher and lower angles teeth in order to avoid any intersection.
Table 1 illustrates the values of these coefficients.

Tab.1. Values of the motor parameters

Designations	β	α	r_{did}	p	N_d
Trapezoidal configuration	1	1	0.2	4	6
Sinusoidal configuration	2/3	3/2	0.2	4	6

The coiled rotor axial flux generator structure is illustrated by the Figure 4.

3.2. Geometric parameters of the stator

The Figure 5 presents the different geometric parameters of the stator:

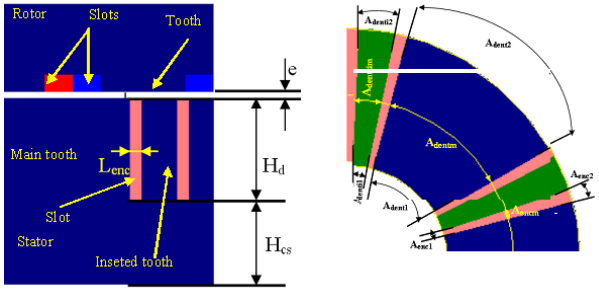

Fig.5. Geometric parameters of the stator

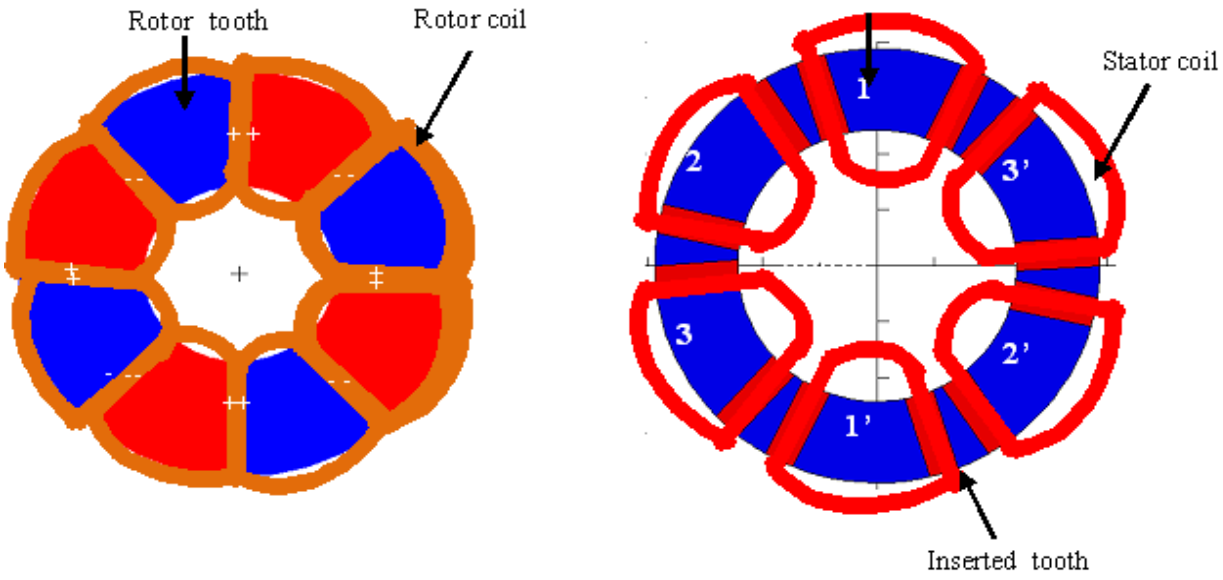

Fig.4. The coiled rotor axial flux generator structure

The slot width is given by the following equation [3-8].

$$L_{enc} = \left(\frac{D_e + D_i}{2}\right)\sin\left(\frac{1}{2}\times\left(\frac{2\times\pi}{N_d} - \alpha\times\beta\times\frac{\pi}{p}\times(1-r_{did})\right)\right) \quad (1)$$

Where D_e and D_i are respectively the external and internal generator diameters, N_d is the number of main teeth and p is the number of poles pairs.

The lower angular width of stator slot is given by the following expression.

$$A_{enc1} = 2\times A\sin\left(\frac{\frac{L_{enc}}{2}}{\frac{D_i}{2}}\right) \quad (2)$$

The superior angular width of stator slot is given by the following expression.

$$A_{enc2} = 2\times A\sin\left(\frac{\frac{L_{enc}}{2}}{\frac{D_e}{2}}\right) \quad (3)$$

The average angular width of a main tooth is expressed as follows.

$$A_{dentm} = \alpha\times\beta\times\frac{\pi}{p} \quad (4)$$

The average angular width of the inserted tooth is expressed as follows.

$$A_{dentim} = r_{did}\times A_{dentm} \quad (5)$$

The average angular width of the slot is expressed as follows.

$$A_{encm} = \frac{1}{2}\times\left(\frac{2\times\pi}{N_d} - A_{dentm} - A_{dentim}\right) \quad (6)$$

The inferior angular width of stator main tooth is given by the following expression.

$$A_{dent1} = A_{dentm} + A_{encm} - A_{dent1} \quad (7)$$

The superior angular width of stator main tooth is given by the following expression.

$$A_{dent2} = A_{dentm} + A_{encm} - A_{dent2} \quad (8)$$

For the configuration with sinusoidal waveforms the height of a tooth is given by the following equation [3-8].

$$H_d = \frac{3\times 2\times N_s}{2\times N_d}\times\frac{\frac{I_{dim}}{\sqrt{2}}}{\delta}\times\frac{1}{K_f}\times\frac{1}{L_{enc}} \quad (9)$$

Where K_f is the filling factor of the slots, δ is the allowable current density in the slots, I_{dim} is the copper conductors sizing current and N_s is the winding turns number.

The calculation method of the dimensioning current is retailed in [3-8].

The heights of the stator yoke are derived by applying the theorem of conservation of flux between the main tooth and the stator yoke [3-5]:

$$H_{cs} = \frac{B_e}{B_{cs}}\times\frac{Min(S_d, S_a)}{2\times\left(\frac{D_e - D_i}{2}\right)} \quad (10)$$

Where B_{cs} is the induction in the rotor yoke, B_e is the flux density in the air-gap, S_d is section of a stator tooth, S_a is the section of the rotor tooth and K_{fu} is the flux leakage coefficient.

3.3. Geometric parameters of the rotor

The Figure 6 presents the different geometric parameters of the rotor.

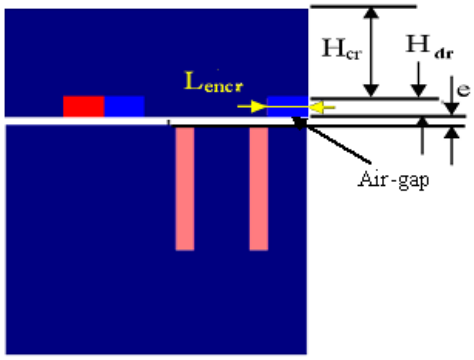

Fig.6. Different geometric parameters of the rotor

The middle width of a rotor slot is expressed by the following equation.

$$A_{encmr} = \gamma\times L_a \quad (11)$$

The rotor slot width is given by the following equation [4, 5].

$$L_{encr} = \left(\frac{D_e + D_i}{2}\right)\sin\left(\frac{A_{encmr}}{2}\right) \quad (12)$$

$$L_a = \frac{\pi}{p}\times\beta \quad (13)$$

With L_a is the middle angular width of the rotor coil and γ is a coefficient adjusted by finite element simulations with the help of the software Maxwell 2D and can be optimized.

The average angular width of the rotor main tooth is expressed as follows:

$$A_{dentmr} = \beta\times\frac{\pi}{p}\times(1-2\times\gamma) \quad (14)$$

The lower angular width of rotor slot is given by the following expression.

$$A_{encr1} = 2\times A\sin\left(\frac{\frac{L_{encr}}{2}}{\frac{D_i}{2}}\right) \quad (15)$$

The superior angular width of rotor slot is given by the following expression.

$$A_{encr2} = 2 \times A \sin\left(\frac{\frac{L_{encr}}{2}}{\frac{D_e}{2}}\right) \quad (16)$$

The height of a rotor tooth H_{dr} permitting to reserve the necessary space for the copper

$$H_{dr} = \frac{n \times I_e}{\delta \times L_{encr}} \quad (17)$$

Where n is the number of rotor coil spire, I_e is the excitation current and δ is the admissible current density in the copper.

The heights of the rotor yoke is derived by applying the theorem of conservation of flux between a magnet or rotor tooth and the rotor yoke [3-58].

$$H_{cr} = \frac{B_e}{B_{cr}} \times \frac{Min(S_d, S_a)}{2 \times \left(\frac{D_e - D_i}{2}\right)} \times \frac{1}{K_{fu}} \quad (18)$$

Where B_{cr} is the magnetic induction in the rotor yoke.

4. Monitoring strategy

The energy generating system allows continuous and secure recovery of energy. Indeed, to a high speed adjustable brake torque or current regulator is applied to regulate the charging current of the batteries. For the first case, braking torque is generated by means of an electromagnet controlled by voltage pulses modulated in pulse width to adjust the braking torque to a value setting the speed of the generator relative to the maximum permissible current. For the second case, charging voltage is adjusted by DC-DC elevator controlled in current by pulse width modulation technique. For the two cases, the control signal of the electromagnet or the DC-DC elevator are find by comparing the reference battery load current fixed to 2600 A to the load current. The comparator output drives a proportional-integral regulator type. The output of the proportional-integral is compared with a triangular wave signal with high frequency. The comparator output drives a hysteresis reproducing the control signal of the electromagnet.

5. Model of the Battery

The energy accumulator is a connecting of battery elementary modules in series and in parallel so as to have a nominal voltage and a power storage capacity set by the specifications. The accumulator model chosen for this study is the Tevenin model (Figure 7) [3, 4]. Model parameters of the energy accumulator are determined by the following tests.

- Direct measurement of the rated battery voltage with a voltmeter.
- Measure of the internal resistance of the battery with a volt-ampere-metric test by connecting the battery to a resistive load.
- Measuring the capacity and resistance of the transitional regime by connecting the battery to a sinusoidal voltage via a protective resistor.

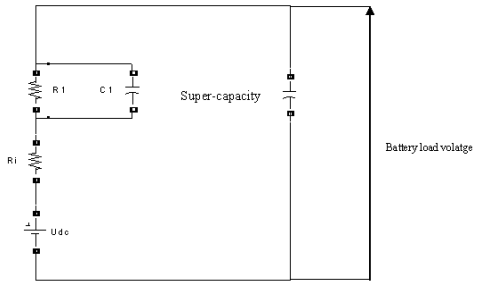

Fig.7. Simulink model of the batteries

R_1 and C_1 are the resistance and the capacity taking into account the transitional arrangements.

R_i is the internal resistance of the battery.

6. Equation of motion

The equation that governs the motion of the rotating parts of the energy generation chain is derived from the fundamental dynamics relationship:

$$J \times \frac{d\Omega}{dt} = T_m - r_d \times (T_{em} - sgn(T_{em}) \times T_{mec} - sgn(T_{em}) \times T_{fer}) - T_c \quad (19)$$

Where J is the moment of inertia of the rotating parts, r_d is the speed amplification ratio, T_m is the torque imposed on the motor shaft caused by the movement of wind, T_{em} is the electromagnetic torque, T_{mec} is the torque due the mechanical losses, T_{fer} is the torque due to iron losses and T_c is the braking torque [4-22]. For the power chain with current regulator the braking torque is set to zero.

$$T_m = \frac{1.918 \times R_p^2 \times V_{vent}^3}{\Omega} \quad (20)$$

$$T_{em} = \frac{1}{\Omega} \sum_{i=1}^{3} e_i \times i_i \quad (21)$$

Where e_i and i_i are respectively the induced electromotive force and the current of the phase i.

Where 1.918 is a coefficient that depends on the kinetic energy of the wind and pale properties, R_p is the pale ray and V_{vent} is the wind speed.

The implementation of this equation in the environment MATLAB / Simulink is illustrated in Figure 8:

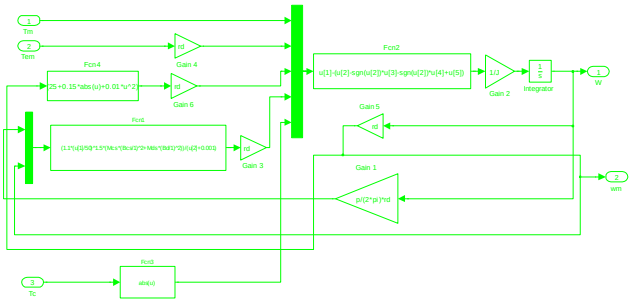

Fig.8. Simulink model of the motion equation

7. Model of the electromotive forces

The three induced electromotive forces are estimated from the following three equations [4-22]:

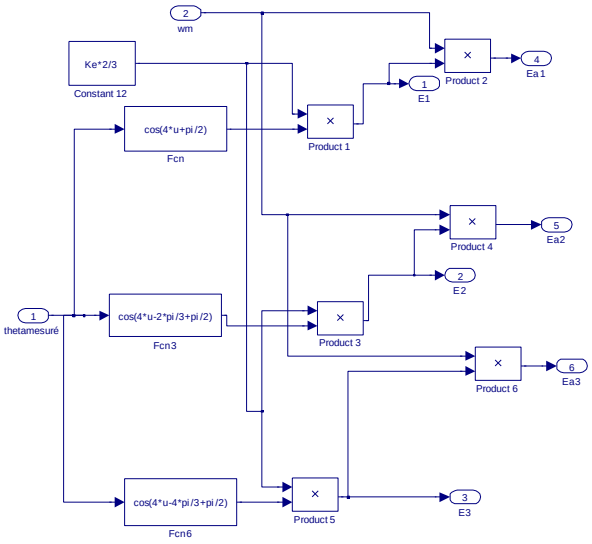

Fig.9. Simulink Model of the electromotive forces

$$e_1 = \frac{2}{3} \times K_e \times \Omega \times \cos\left(p \times \Omega \times t + \frac{\pi}{2} \right) \quad (22)$$

$$e_2 = \frac{2}{3} \times K_e \times \Omega \times \cos\left(p \times \Omega \times t - \frac{2 \times \pi}{3} + \frac{\pi}{2} \right) \quad (23)$$

$$e_3 = \frac{2}{3} \times K_e \times \Omega \times \cos\left(p \times \Omega \times t - \frac{4 \times \pi}{3} + \frac{\pi}{2} \right) \quad (24)$$

Where K_e is the electromotive constant, Ω is the angular velocity of the generator and p is the number of pole pairs.

The Simulink model of the electromotive forces is illustrated by the Figure 9:

8. Model of the AC-DC conversion chains

The generator phase voltages are given by the following relationships [6-14]:

$$v_1 = R \times i_1 + (L - M) \times \frac{di_1}{dt} + e_1 \quad (25)$$

$$v_2 = R \times i_2 + (L - M) \times \frac{di_2}{dt} + e_2 \quad (26)$$

$$v_3 = R \times i_3 + (L - M) \times \frac{di_3}{dt} + e_3 \quad (27)$$

Where R, L and M are respectively the phase resistance, phase inductance and phase mutual inductance.

The three phase voltages are converted into a DC voltage through a three phase rectifier. The rectified voltage is filtered by a capacitor. The output voltage of the rectifier attacks directly the batteries for recharging. For the power chain with current regulator a DC-DC elevator is added to protect the power chain.

The Simulink model of the generator-rectifier-Batteries assembly is shown in Figure 10 [3, 4].

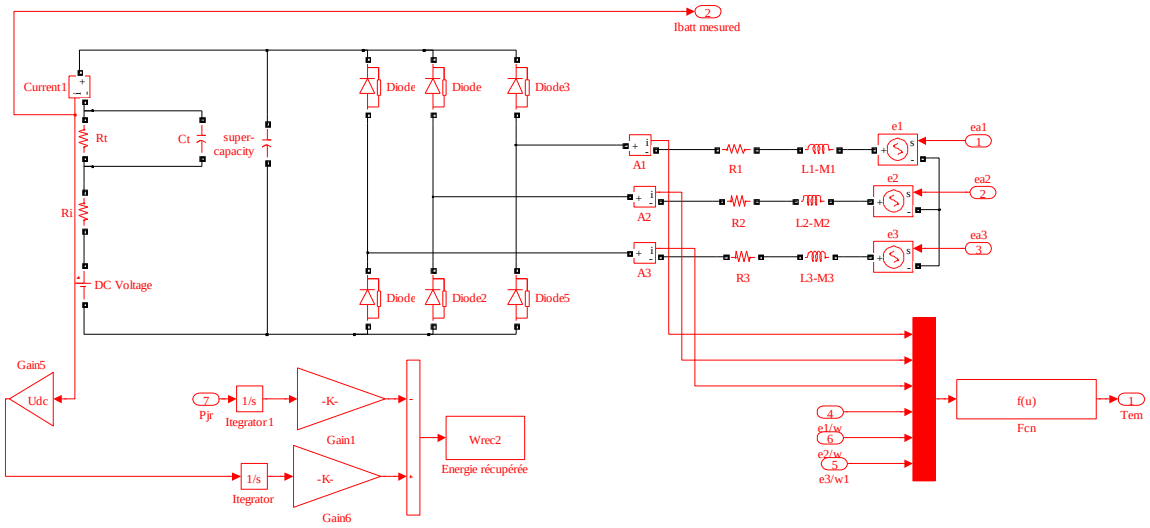

Fig.10. Simulink model of the generator-rectifier-Batteries assembly

The Simulink model of the generator-rectifier-DC/DC elevator-Batteries assembly is shown in Figure 11 [3, 4].

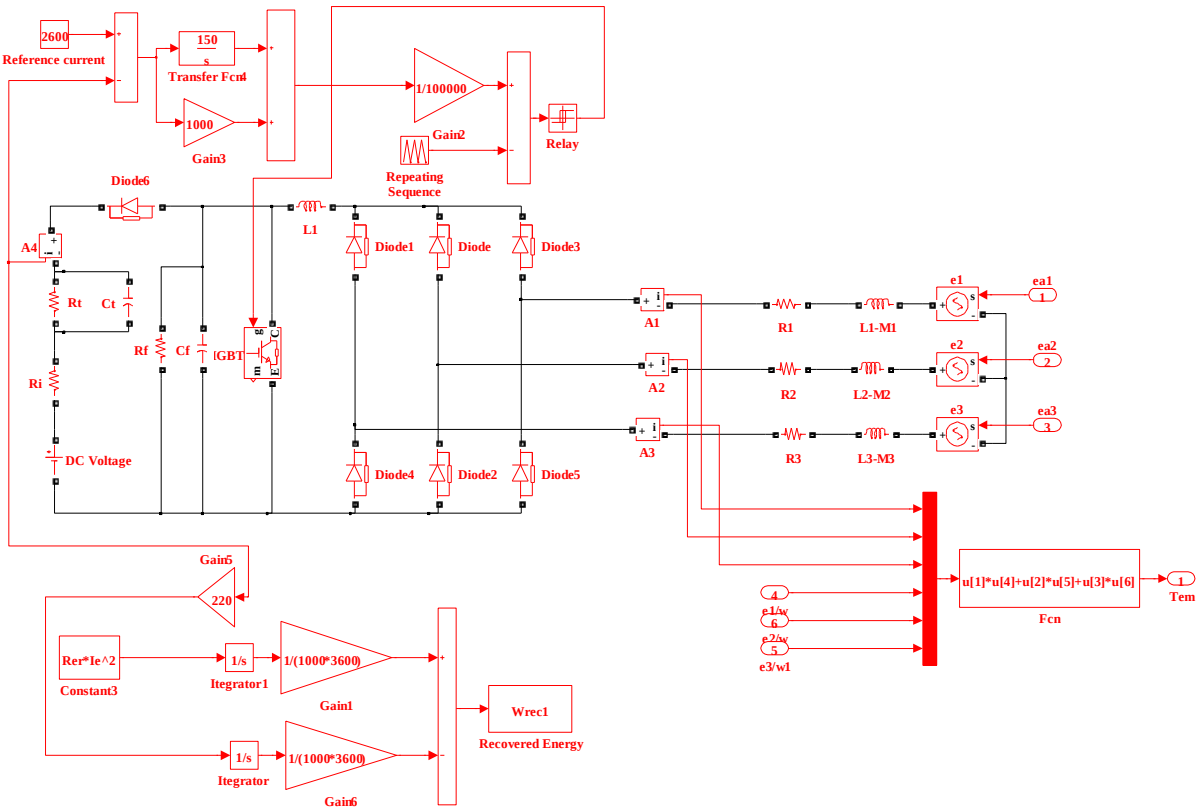

Fig.11. Simulink model of the generator-rectifier-DC/DC elevator-Batteries assembly

9. Current regulator

The batteries current regulator (Figure 12) limits the batteries charging current to a value equal to 2600 A, to protect the energy generation chain against the burn. This value is held into account by the design approach of the power chain [3, 4]. Indeed, the charging reference current is compared to the charging measured current. The output of the comparator attacks a proportional integral regulator. The output of the regulator attacks a hysteresis varying between 0 and 1to generate the control signal of the DC-DC elevator inverter supplying the battery.

The excitation current regulator system (Figure 13) permit to regulate the excitation current to limits the charging current to 2600 A. Indeed, the charging reference current is compared to the charging measured current. The output of the comparator attacks a proportional integral regulator. The output of the regulator attacks a hysteresis varying between 0 and 1to generate the control signal of the DC-DC elevator inverter supplying the excitation winding.

The braking system (Figure 14) also limits the batteries charging current to the same value (2600 A), to protect the energy generation chain via a proportional integral regulator producing the control signal of the electromagnet.

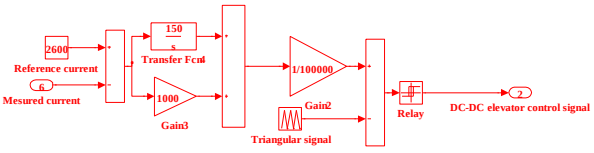

Fig.12. Recharge current regulator via DC-DC elevator

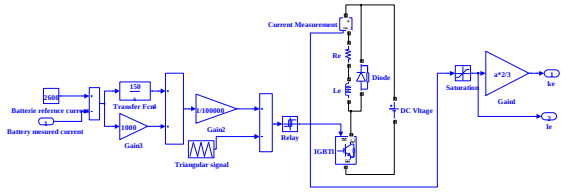

Fig.13. Excitation current regulator

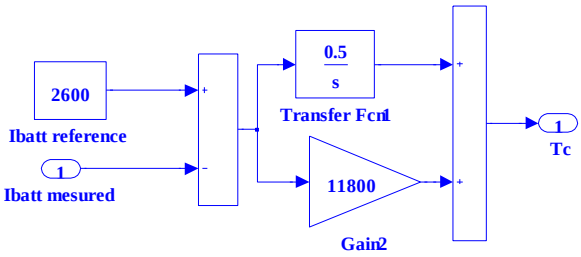

Fig.14.Braking torque regulator

10. Global model of the power chain

The global model of the energy generation system for the three cases is based on the connection of the different Simulink models of the chain components make up this chain according to Figure 15, Figure 16 and Figure 17 [3-5]:

11. Description of Simulation Results

Simulation parameters calculated from a generator sizing program are illustrated in Table 2 [12-22].

Tab.2. Simulation parameters

Nomenclatures	Values	Units
Phase resistance (R)	0.882	mΩ
Phase inductance (L)	2.247098	mH
Mutual inductance (M)	0.841539	mH
Moment of inertia of the rotating parts (J)	25081.455	Kg.m^2
Supper capacity (C)	15	Farads
internal resistance of the battery (Ri)	0.02	Ω
Resistance modeling the transitional arrangements for charging and discharging of batteries indentified by experimental test (R1)	0.001	Ω
Capacity modeling the transitional arrangements for charging and discharging of batteries indentified by experimental test (C1)	1	Farad
Gear ratio (rd)	8	/
Batteries nominal voltage (Udc)	220	Volts
Inductor inductance (Le)	41.880	mH
Inductor resistance (Re)	0.295	Ω

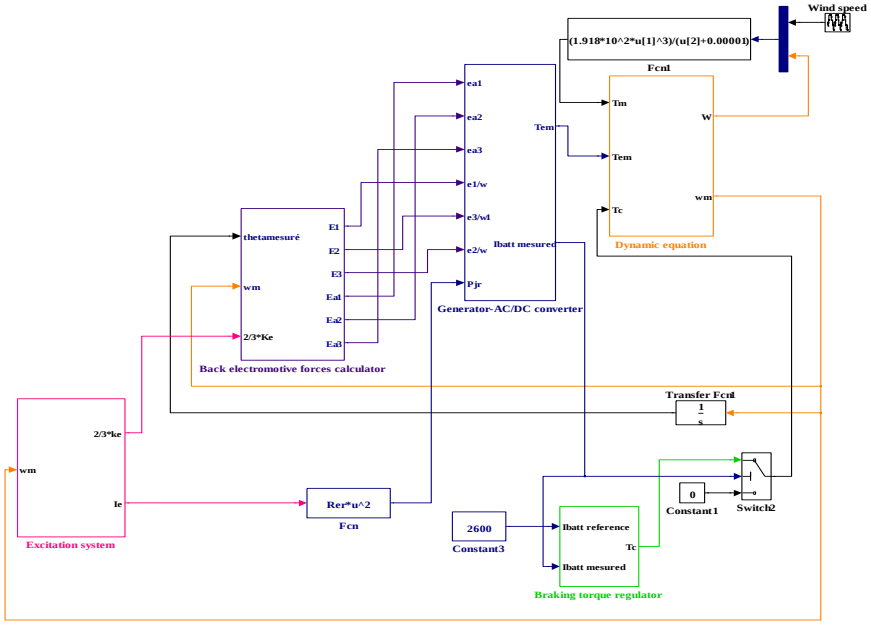

Fig.15. Simulink model of the global energy generation chain with braking system

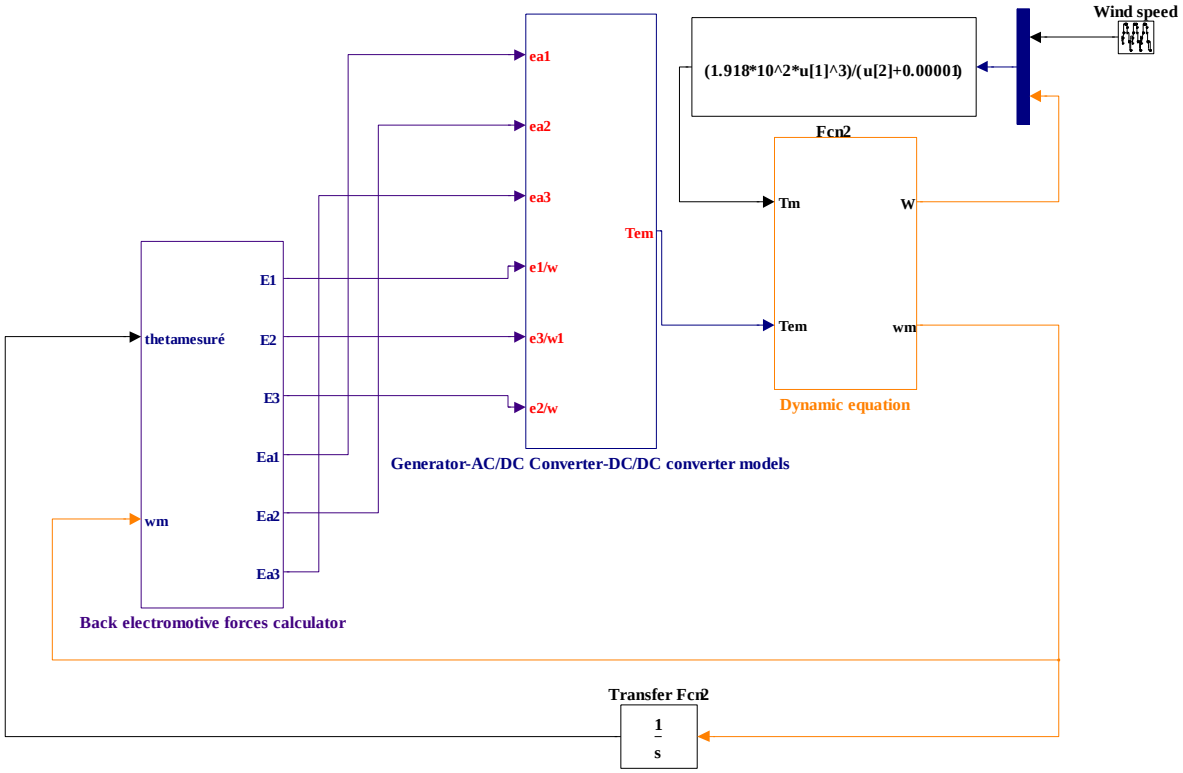

Fig.16. Simulink model of the global energy generation chain with current regulator

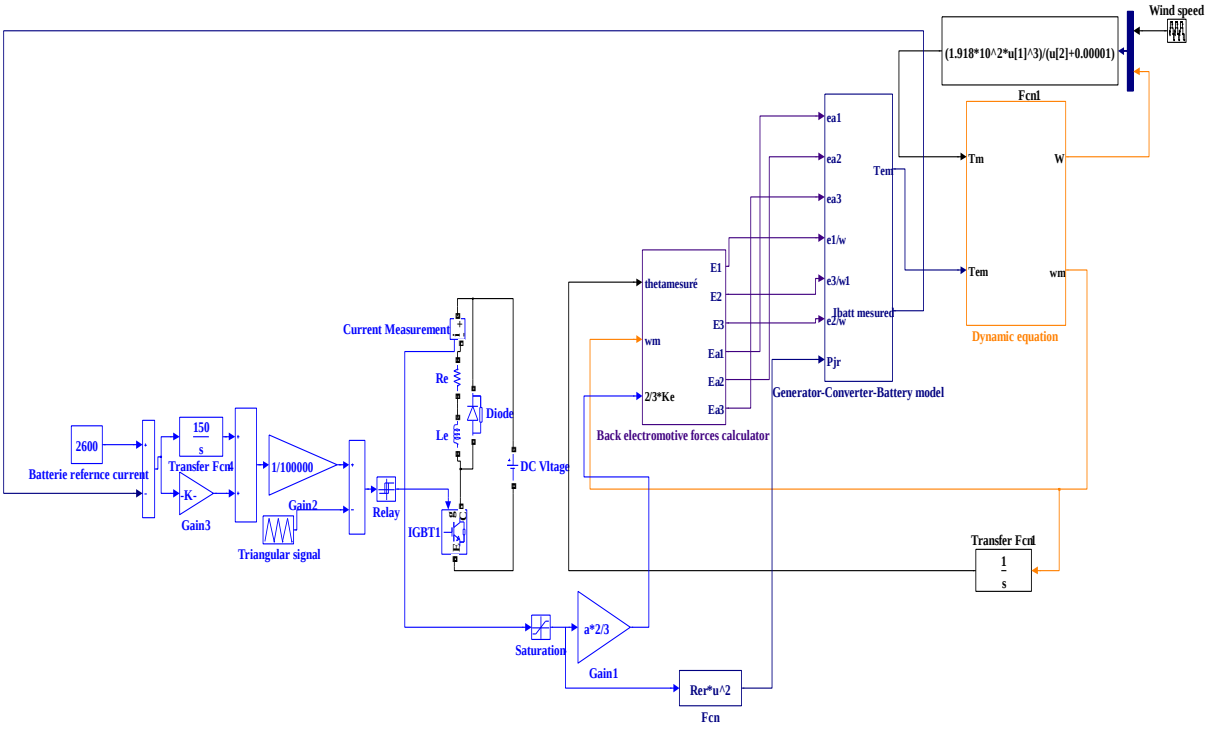

Fig.17. Simulink model of the global energy generation chain with excitation current regulator

Figure 18 shows the wind speed profile.

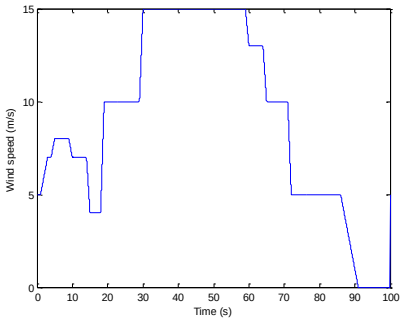

Fig.18. Wind speed profile

The pace of this speed is chosen randomly and strongly with operating constraints such as speed limit, to test the performance of the control algorithm of the energy generation chain.
The angular speeds of the generator for the three power chain structures are illustrated by the Figure 19:

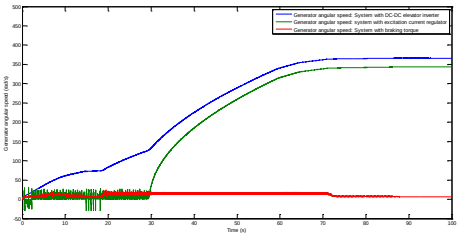

Fig.19.Generator angular speed for the three power chains structures

Figure 19 shows that after training in movement of the generator shaft, the wind stopping does not immediately causes the stop of the generator shaft as a result of the inertia of the rotating parts. For the same speed cycle of the propeller, the speed of the generator shaft is greatly reduced for the case of structure with mechanical brake by the brake action compared to the other structures. By consequence, for the configurations with current regulator and excitation current regulator, the speed is higher as the battery charging current is reduced by current regulation, not by mechanical brake.
Figure 20 shows the evolutions electromotive forces induced by the generator for the two structures.

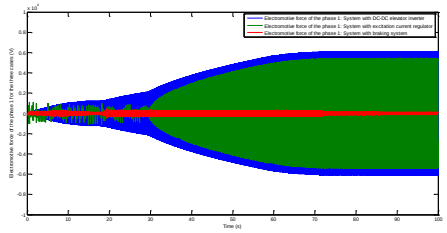

a. Evolution of the electromotive forces

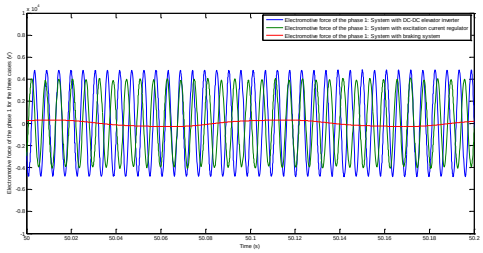

b. Zoom of the evolution of the electromotive forces

Fig.20. Induced electromotive forces for the three configurations

Figure 20 shows that the amplitude of the electromotive forces is relatively high for the systems with current DC-DC elevator and with excitation current regulator relating the other configuration, because the difference in angular speed of the shaft for the three configurations. For the three cases, the important values of the electromotive forces is explained by the insertion of a gear amplifier with amplifying ratio $r_d = 8$. This is to compensate the drop of phase voltages of the generator at battery charging phase.
Figure 21 illustrates the phase currents generated by the two generators.

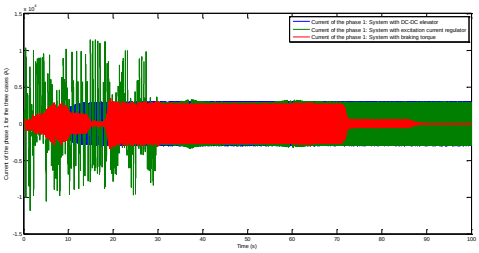

a. Evolution of the current of the phase 1 for the three cases

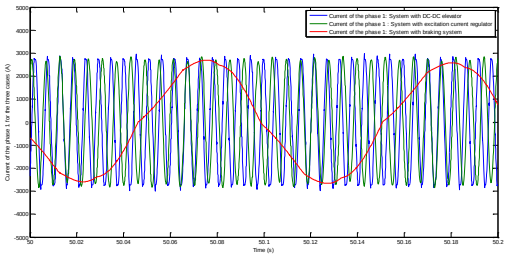

b. Zoom of the evolution of the current of the phase 1 for the three cases

Fig.21. Phase currents of the generator for the three configurations

Figure 21 shows that the amplitude of the generator phase currents depends primarily on the internal resistance of the battery and of the rectified voltage. The amplitude of phases currents for the three cases of configuration are comparable leading to the setting in equivalence of the three structures point of

view energy recuperation.
For the configuration with excitation current regulation system the evolution of the excitation current is illustrated by Figure 22.

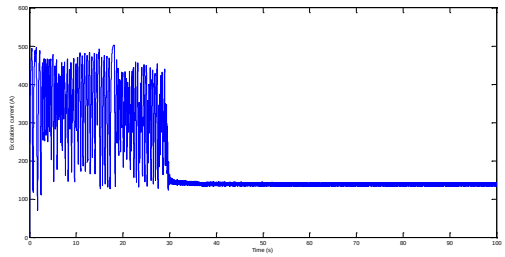

Fig.22. Evolution of the excitation current for the configuration with excitation current regulator

Figure 22 shows the stabilisation of the excitation when the charging current is near to 2600 A. At the stat, the fluctuation of the excitation depend on the dynamic of the global system et the fact to impose a charging current equal to 2600 A.
For the configuration with braking torque system, the evolution of the braking torque is illustrated by the figure 23.

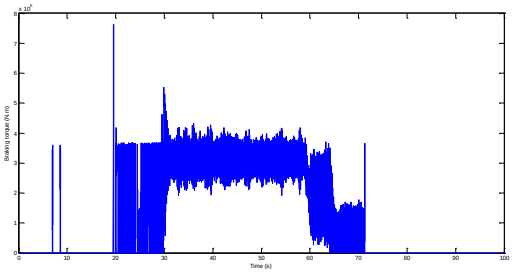

Fig.23. Evolution of the braking torque

The figure 23 shows that the braking torque is high for high speed values, which is explained by the fact that the battery charging current is regulated to a reference value equal to 2600 A.
For the three configurations, the battery charging voltage is shown in Figure 24.

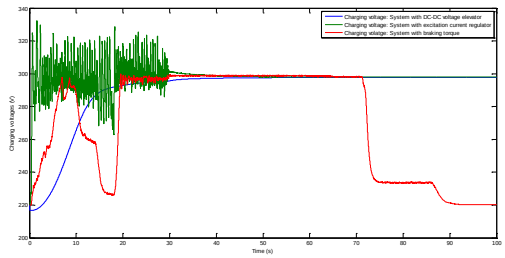

Fig.24. Battery charging voltage for the three configurations

For the configurations with DC-DC elevator inverter and with excitation current regulator, Figure 24 shows that the charging voltage is maintained continuously. This confirms the effectiveness of these configurations. The amplitude of this voltage allows a continuous charging of the batteries as the nominal battery voltage is 220V significantly below to this voltage for these configurations. For the configuration with braking torque there are areas of discontinuity showing the poor performance of this configuration regarding to the two others configurations.
For the three configurations, the batteries charging current is shown in Figure 25.

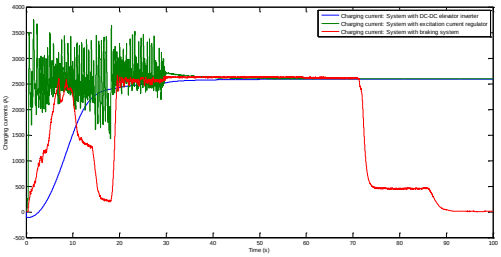

Fig.25. Battery charging current for the three cases

For the configurations with DC-DC elevator inverter and with excitation current regulator, Figure 25 shows that the charging current is maintained continuously. This confirms the effectiveness of these configurations. The change versus time of this current allows a continuous charging of the batteries as the nominal battery voltage is 220V significantly below to the charging voltages for these configurations. For the configuration with braking torque, there are areas of discontinuity, showing the poor performance of this configuration regarding to the two others configurations.
The power generated by the wind and the powers recovered by the batteries for the three cases are illustrated by the Figure 26.

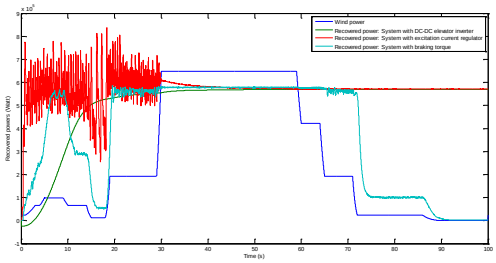

Fig.26. Wind and recovered powers

The Figure 26 show that the power transferred to the batteries is lower than that developed by the wind, which is explained by the different losses of energy generation chain. Also this figure shows that the power chains with excitation current regulator and with DC-DC elevator ensures a continuous energy recovery.
For the three configurations, the energy recovered by the batteries is shown in Figure 27.

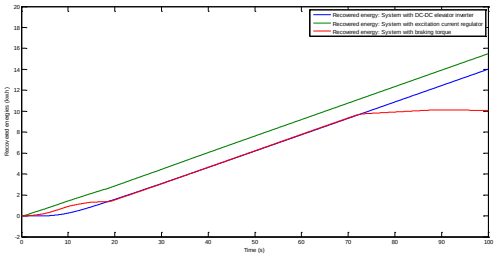

Fig.27. The energy recovered by the batteries

This recovered energy is approximately equal to 14 kw.h for the power chain with current DC-DC elevator, 10 kw.h for the power chain with braking system and 15.75 kw. For the power chain with excitation current regulator important values which validates the performance of the two three control algorithms. This difference is caused by the fact that the power chains with DC-DC elevator inverter and with excitation current regulator ensures a continuous energy recovery.

The configuration with excitation current regulator is less expensive and can recover the most elevated energy compared to the other two configurations. It has the simplest control algorithm as a simple structure. It is then chosen as the means for generating renewable energy.

12. Conclusion

In this paper is presented a design and control models of a generation chain of renewable energy based on the choice of the structure and components of this power chain jointly optimizing the cost and recovered energy. A comparative study between three protection systems with DC-DC elevator inverter regulator, with mechanical brake and the other with excitation current regulator led to the selection of the configuration with excitation current regulator because it is less expensive and can recover the most elevated energy compared to the other two configurations. It also has the simplest control algorithm as a simple structure. It is then chosen as the means for generating renewable energy. Simulation results are encouraging and validate completely the design and control approach of the generation of renewable energy chain.

As perspective, it will be interesting to industrialize this innovated structure of renewable energy generation.

References

1. Faten Grouz, Lassad Sbita, Mohamed Boussak and Amor Khalief, FDI based on an adaptive observer for current and speed sensors of PMSM drives. Simulation Modelling Practice and Theory, vol. 35, pp. 34-49, 2013.
2. HT Jadhav and Rajit Roy, A comprehensive review on the grid integration of doubly fed induction generator. International Journal of Electrical Power and Energy Systems, vol. 49, pp. 8-18, 2013.
3. Souhir Tounsi, Design and Optimization of Axial Flux Brushless DC Generator Dedicated to Generation of Renewable Energy, American Journal of Electrical Power and Energy Systems. Special Issue:Design and Monitoring of Renewable Energy Systems (DMRES). Vol. 4, No. 3-1, 2015, pp. 1-5. doi: 10.11648/j.epes.s.2015040301.11.
4. Wiem Nhidi, Souhir Tounsi, Mohamed Salim Bouhlel, Design and Modeling of a Synchronous Renewable Energy Generation System, American Journal of Electrical Power and Energy Systems. Special Issue:Design and Monitoring of Renewable Energy Systems (DMRES). Vol. 4, No. 3-1, 2015, pp. 6-11. doi: 10.11648/j.epes.s.2015040301.12.
5. Mariem Ben Amor, Souhir Tounsi, Mohamed Salim Bouhlel, Design and Optimization of Axial Flux Brushless DC Motor Dedicated to Electric Traction, American Journal of Electrical Power and Energy Systems. Special Issue:Design, Optimization and Control of Electric Vehicles: (DOCEV). Vol. 4, No. 2-1, 2015, pp. 42-48. doi: 10.11648/j.epes.s.2015040201.16.
6. Chaithongsuk, S., Nahid-Mobarakeh, B., Caron, J., Takorabet, N., & Meibody-Tabar, F. : Optimal design of permanent magnet motors to improve field-weakening performances in variable speed drives. Industrial Electronics, IEEE Transactions on, vol 59 no 6, p. 2484-2494, 2012.
7. Rahman, M. A., Osheiba, A. M., Kurihara, K., Jabbar, M. A., Ping, H. W., Wang, K., & Zubayer, H. M. : Advances on single-phase line-start high efficiency interior permanent magnet motors. Industrial Electronics, IEEE Transactions on, vol 59 no 3, p. 1333-1345, 2012.
8. C.C Hwang, J.J. Chang : Design and analysis of a high power density and high efficiency permanent magnet DC motor, Journal of Magnetism and Magnetic Materials, Volume 209, Number 1, February 2000, pp. 234-236(3)-Publisher: Elsevier.
9. MI. Chunting CHRIS : Analytical design of permanent-magnet traction-drive motors" Magnetics, IEEE Transactions on Volume 42,

Issue 7, July 2006 Page(s):1861 - 1866 Digital Object Dentifier 10.1109/TMAG.2006.874511.
10. S.TOUNSI, R.NÉJI, F.SELLAMI : Conception d'un actionneur à aimants permanents pour véhicules électriques, Revue Internationale de Génie Électrique volume 9/6 2006 - pp.693-718.
11. Sid Ali. RANDI : Conception systématique de chaînes de traction synchrones pour véhicule électrique à large gamme de vitesse. Thèse de Doctorat 2003, Institut National Polytechnique de Toulouse, UMRCNRS N° 5828.
12. C. PERTUZA : Contribution à la définition de moteurs à aimants permanents pour un véhicule électrique routier. Thèse de docteur de l'Institut National Polytechnique de Toulouse, Février 1996.
13. S. TOUNSI, R. NEJI and F. SELLAMI: Mathematical model of the electric vehicle autonomy. ICEM2006 (16th International Conference on Electrical Machines), 2-5 September 2006 Chania-Greece, CD: PTM4-1.
14. R. NEJI, S. TOUNSI, F. SELLAMI: Contribution to the definition of a permanent magnet motor with reduced production cost for the electrical vehicle propulsion. Journal European Transactions on Electrical Power (ETEP), Volume 16, issue 4, 2006, pp. 437-460.
15. Aicha Khlissa, Houcine Marouani, Souhir Tounsi, Systemic Design and Modelling of a Coiled Rotor Synchronous Motor Dedicated to Electric Traction, American Journal of Electrical Power and Energy Systems. Special Issue:Design, Optimization and Control of Electric Vehicles: (DOCEV). Vol. 4, No. 2-1, 2015, pp. 1-7. doi: 10.11648/j.epes.s.2015040201.11.
16. Houcine MAROUANI and Souhir TOUNSI : Design of a Coiled Rotor Synchronous Motor Dedicated to Electric Traction. Journal of Electrical Systems (JES), Volume 10, Issue 3, (September 2014), Indexed in SCOPUS.
17. Ajmia BEGACEM, Mohamed Amine FAKHFAKH and SouhirTOUNSI : « OPTIMAL DESIGN AND CONTROL OF ELECTRIC VEHICLE POWER CHAIN » Journal of Electrical Engineering (JEE), Edition 2, juin 2015, Indexed in SCOPUS.
18. S.TOUNSI:"Losses modelling of the electromagnetic and IGBTs converters", International Int. J. Electric and Hybrid Vehicles (IJEHV)-Indersciences publisher, Vol. 5, No. 1, 2013, pp: 54-68.
19. Amal Suilah, Nadia Graja, Amal Boudaya, Souhir Tounsi, Modelling of Synchronous Generation System for Renewable Energy, International Journal of Electrical Components and Energy Conversion. Vol. 1, No. 1, 2015, pp. 36-43. doi: 10.11648/j.ijecec.20150101.14.
20. Marwa Sellami, Souhir Tounsi. Control of Axial Flux DC Motor with Permanent Magnet Dedicated to Electric Traction.International Journal of Electrical Components and Energy Conversion. Vol. 1, No. 1, 2015, pp. 44-48. doi:10.11648/j.ijecec.20150101.15.
21. Moez Hadj Kacem, Souhir Tounsi, Rafik Neji. Losses Modeling of the Electric Vehicles Power Chain. International Journal of Electrical Components and Energy Conversion. Vol. 1, No. 2, 2015, pp. 49-54. doi: 10.11648/j.ijecec.20150102.11.
22. S. TOUNSI , N. Ben Hadj, R. and F. Sellami Neji: "Optimization of Electric Motor Design Parameters Maximizing the autonomy of electric vehicles", International Review of Electrical Engineering (IREE), ISSN 1827-6660, Volume 2 No. 1, January-February 2007, pp. 118-126, Indexed in SCOPUS.